Applied Catalysis B: Environmental 160–161 (2014) 279–285

Contents lists available at ScienceDirect

Applied Catalysis B: Environmental

journal homepage: www.elsevier.com/locate/apcatb

Fabrication of positively and negatively charged, double-shelled, nanostructured hollow spheres for photodegradation of cationic and anionic aromatic pollutants under sunlight irradiation☆

Shunxing Li[a,b,*], Jiabai Cai[a], Xueqing Wu[a], Fengying Zheng[a,b], Xiaofeng Lin[a], Wenjie Liang[a], Jie Chen[a], Jianzhong Zheng[a], Zhanghua Lai[a], Tanju Chen[a], Licong Zhu[a]

[a] College of Chemistry and Environment, Minnan Normal University, Zhangzhou, 363000, China
[b] Fujian Province Key Laboratory of Modern Analytical Science and Separation Technology, Minnan Normal University, Zhangzhou, 363000, China

ARTICLE INFO

Article history:
Received 28 February 2014
Received in revised form 6 May 2014
Accepted 11 May 2014
Available online 16 May 2014

Keywords:
Positively and negatively charged
Double-shelled nanomaterials
Sunlight
Photocatalysis

ABSTRACT

A novel approach to prepare double-shelled, nanostructured hollow spheres with positively and negatively charged was proposed. If the difference in isoelectric points between M_xO and N_yO was large enough, at a certain pH range, the inner and outer shell of double-shelled $M_xO@N_yO$ hollow spheres were positively and negatively charged, respectively. A proof-of-concept was shown, using WO_3 and TiO_2 as anionic and cationic building subunits, respectively. The nanoparticles of WO_3 and TiO_2 were coated successively onto the functionalized polystyrene (PS) template beads, the resulted $PS@WO_3@TiO_2$ nanocomposites were calcined at elevated temperature, and then double-shelled $WO_3@TiO_2$ hollow spheres were obtained. The dispersity, morphology, size, and lattice of these hollow spheres were tested by scanning electron microscopy (SEM) and transmission electron microscopy (TEM). The presence and purity of both WO_3 and TiO_2 phases were confirmed by electron energy loss mapping analysis and X-ray diffraction analysis (XRD). The specific surface area and the average pore diameter of these hollow spheres were 53.04 m^2/g and 8.042 nm, respectively. The photocatalytic activity for the degradation of cationic and anionic aromatic pollutants was in the order of double-shell hollow spheres $WO_3@TiO_2$ > single-shell WO_3-TiO_2 > P25, i.e., the synergistic effect of coupling TiO_2 with WO_3 on photocatalytic performance was proved by us.

1. Introduction

In recent years, sunlight driven photocatalysis plays an important role in dealing with organic pollutants [1–3]. Both anionic and cationic organic pollutants are coexisted in the wastewater. In the development of nanostructured photocatalysts, three key obstacles should be overcome, including the separation of photoexcited electrons and holes [4], the residence time of the light on/in the photocatalyst [5,6], and the simultaneous degradation of anionic and cationic organic pollutants. Such challenges can be unlocked by structural and morphological innovations [7–9], e.g., the structure of hollow spheres has been used to solve the first two obstacles [10,11]. If the inner and outer surface charges of hollow spheres are positive and negative, respectively, the affinity between anionic and cationic pollutants and the photocatalyst will be enhanced, and then the major obstacle of heterogeneous photocatalysis (i.e., the poor surface coverage of pollutants on the photocatalyst) can be resolved. Therefore, it is necessary to develop double-shelled hollow spheres with positively and negatively charged for the photodegradation of anionic and cationic organic pollutants.

Herein, we present a novel, simple, and general method for preparing such photocatalysts. Using polystyrene spheres (PS) with negatively charged as sacrificial templates, metal ions with positively charged could be adsorbed onto PS. After oxidation and hydrolysis, metal oxide (denoted as M_xO) were formed and coated onto PS. The surface hydroxyl from M_xO could be used for the coordination of the other metal (denoted as N). After calcination at high temperature, double-shelled $M_xO@N_yO$ hollow spheres could be obtained. If the difference of the isoelectric point between M_xO and

☆ Electronic supplementary information (ESI) available: SEM and TEM images, XRD pattern, EDX data, TG data, FTIR spectra, nitrogen adsorption–desorption isotherm, surface area, and porosity measurements of $WO_3@TiO_2$ hollow spheres, correlation coefficient R^2, and isoelectric point of nanometer semiconductors.

* Corresponding author at: Corresponding author at: Fujian Province Key Laboratory of Modern Analytical Science and Separation Technology, Minnan Normal University, Zhangzhou, 363000, China. Tel.: +86 596 2591395; fax: +86 596 2591395.
E-mail address: shunxing.li@aliyun.com (S. Li).

http://dx.doi.org/10.1016/j.apcatb.2014.05.021
0926-3373/

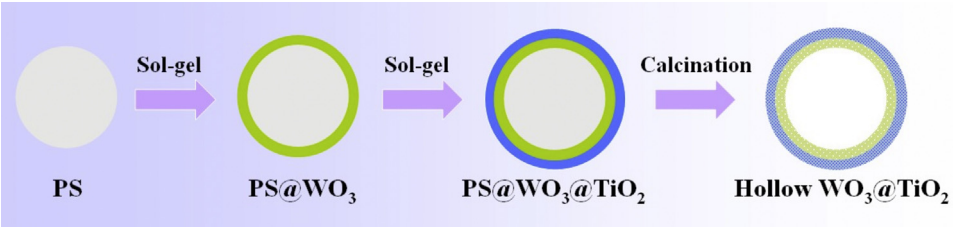

Scheme 1. Scheme of fabrication of the monodisperse double-shelled WO_3@TiO_2 hollow spheres using the "template + sol–gel + calcination" method.

N_yO was large enough, the inner and outer shell of M_xO@N_yO hollow spheres would carry a net positively and negatively charged, respectively, at a certain pH range (Scheme 1). A proof-of-concept was shown, using tungsten trioxide (WO_3) and titanium dioxide (TiO_2) as cationic and anionic building subunits, respectively, because the isoelectric point is 0.4 for WO_3 and 6.2 for TiO_2 [12]. With a band gap of 2.7 eV, WO_3 is a promising visible-light-responsive photocatalyst for the degradation of organic pollutants [13,14]. As well, TiO_2 has been widely used as a photocatalyst for its relatively high photocatalytic activity, wide band gap (3.2 eV), low cost, low toxicity, and high chemical stability [15–17]. Therefore, some studies have reported on the core–shell WO_3-TiO_2 spheroids [18,19], WO_3-TiO_2 films [20,21], TiO_2-WO_3 nanotubes [22–24], WO_3-TiO_2 nanorod arrays [25,26], and WO_3-TiO_2 nanowires [27], and single-shelled WO_3-TiO_2 hollow spheres [28]. Despite intense efforts in WO_3-TiO_2 nanocomposites, WO_3@TiO_2 hollow spheres with new structural characteristics of double-shelled and surface positively and negatively charged have not been proposed yet.

2. Experimental

2.1. Reagents and chemicals

Tetrabutyl titanate (TBOT, J&K, 99%), tungsten hexachloride (WCl_6, Aladdin), sodium persulfate (Xilong, 98%), and ethanol (Xilong, 99.7%) were purchased in China and used without additional purification. Methyl acrylate (Sinopharm, 98%) and styrene (Sinopharm, 99%) were used after passing through the inhibitor removal column and vacuum distillation. Distilled water was employed as the polymerization medium.

2.2. Synthesis of PS spheres

According to a modified method [29], PS spheres were prepared by the interpolymer interactions between styrene and methyl acrylate. A double-neck and round-bottom flask equipped with reflux condenser, mechanical agitation, temperature controller, and N_2 agitation was used as reactor. The air in the reactor was replaced by a steam of N_2 and then the reaction system was kept under N_2 until the polymerization was finished. After adding 85 mL of distilled water, 10.47 mL of styrene, and 0.52 mL of methyl acrylate, the reactor was heated and maintained at 70 °C, the solution of sodium persulfate (0.15 g in 5 mL of water) was added to start the polymerization process for 24 h, and then PS as latex with ca. 10% solid content were collected.

2.3. Synthesis of PS@WO_3, PS@TiO_2, and PS@WO_3-TiO_2 particles

WCl_6 (0.2 mmol) was dissolved in 20 mL of ethanol, forming a 0.01 mol/L solution. As core template, 0.25 g of PS was uniformly dispersed by ultrasonication in 50 mL of ethanol. The WCl_6 solution was added at a speed of 10 s per drop under vigorous stirring, and then kept for 20 h. After removing the solvent by the centrifugation, the resulting PS@WO_3 was washed three times with ethanol and dried in vacuum at 60 °C for 6 h. Using TBOT (0.6 mmol), both WCl_6 (0.06 mmol) and TBOT (0.6 mmol) as the precursors, respectively, PS@TiO_2 and PS@WO_3-TiO_2 sample were also prepared by same method.

2.4. Synthesis of PS@WO_3@TiO_2 particles

In 10 mL of ethanol, TBOT (0.15 mL) was dissolved and then PS@WO_3 (0.03 g) dispersed in the mixture of 0.65 mL of water and 10 mL of ethanol was added. After refluxing at 70 °C for 10 h, obtained PS@WO_3@TiO_2 particles was washed with ethanol by three cycles of centrifugation/redispersion and then dried in vacuum at 60 °C for 6 h.

2.5. Fabrication of single-shelled of WO_3, single-shelled of TiO_2, single-shelled of WO_3-TiO_2, and double-shelled WO_3@TiO_2 hollow spheres

In a conventional muffle furnace, the obtained PS@WO_3@TiO_2 or PS@WO_3 or PS@ TiO_2 or PS@WO_3-TiO_2 particles were heated with a rate of 5 °C/min from room temperature to 550 °C and calcinated at 550 °C for 3 h. The PS were removed and then single-shelled of WO_3, single-shelled of WO_3-TiO_2, and double-shelled WO_3@TiO_2 hollow spheres were finally obtained.

2.6. Characterization

Scanning electron microscopy (SEM) images were carried out on a Gemini microscope (Hitachi, S-4800, Japan) at an accelerating voltage of 10 kV. Prior to analysis, samples were coated with thin Au layer to increase the contrast and quality of the images. Transmission electron microscopy (TEM) images were recorded on FEI America Tecnai G2 F20 U-TWIN microscope operated at 200 kV acceleration voltages. Samples were prepared by drying a drop of the dilute solutions of the particles on a carbon grid. In order to prove the independent presence of WO_3 shell and TiO_2 shell, i.e., double-shelled WO_3@TiO_2 hollow spheres, samples were analyzed by elemental mapping image and EDX analysis on same TEM. In this analysis, when electron beam was incident into a specimen, a part of the electrons was inelastically scattered and lost a fraction of the energy. The distribution of element in a specimen was clarified by selecting and imaging the electrons with a specific energy loss. X-ray scattering patterns (XRD, D/MAX-TTRIII(CBO), Rigaku corporation, Japan) were scanned by analyzing the samples using Cu-Kα monochromatic beam at 40 kV and 30 mA over 20 min rang 20–80. Fourier-transform infrared (FTIR) spectra were recorded with a Perkin Elmer Instruments Co. Ltd. FTIR spectrometer prepared by mixing the samples with KBr. Thermo-gravimetric analysis (TG) was performed on a TG 2009F1 analyzer (NETZSCH, Germany). Before measurements, samples were dried in vacuum for ca. 12 h and then heated with a rate of 15 K/min in porcelain crucibles from 25 °C to 900 °C with nitrogen as carrier gas. The UV–vis absorption spectra were measured using a UV–vis 2550 spectrophotometer (Shimadzu corporation). The system was referenced to a $BaSO_4$ powder

sample prior to collecting data on TiO_2, WO_3, WO_3-TiO_2 and WO_3@TiO_2 hollow spheres. BET surface area measurements were carried out via N_2 adsorption at 77 K using an ASAP2020 instrument based on adsorption data in the partial pressure (P/P_0) range of 0.01–0.99.

2.7. Photocatalytic and adsorptive activity measurements

Fifty milliliter solution (pH 5) of cationic aromatic pollutants (Rhodamine B, methyl violet, or 4-nitroaniline) and anionic aromatic pollutants (methyl orange, acid violet 43, or trimesic acid) was used respectively for the test of photocatalytic and adsorptive activity, which concentration was 20×10^{-3} g/L for methyl orange and 5×10^{-3} g/L for other five kinds of aromatic pollutants. The photocatalysts (30 mg of WO_3, TiO_2, P25, WO_3-TiO_2, or WO_3@TiO_2) with pollutant were stirred in the dark for 1 h to reach the adsorption/desorption equilibrium between the aromatic pollutants and the hollow spheres and then their photocatalytic performances were tested under the irradiation with a 350 W Xenon Short Arc Lamp at room temperature. The light of wavelengths less than 300 nm was filtered with the Pyrex glass to simulate the sunlight [30]. After irradiation for different time intervals, the samples were taken out from aqueous dispersions, the hollow spheres were removed by the filtration, and the concentration of the pollutant was determined by spectrophotometry. The degradation rate could be calculated using Eq. (1).

$$\text{Degradation rate} = 100\% \times \frac{(C_0 - C)}{C_0} \quad (1)$$

Here, C_0 is the initial pollutant concentration before visible light irradiation, and C is the pollutant concentration in the solution after the photodegradation.

The first-order kinetic equation (Eq. (2)) was used to fit the experimental data:

$$\ln\left(\frac{C_0}{C}\right) = k_{app} \times t \quad (2)$$

where k_{app} was the reaction rate constant, and t was the reaction time [31].

The adsorbent (30 mg of WO_3, TiO_2, WO_3-TiO_2, or WO_3@TiO_2) with pollutant were stirred in the dark for different time intervals, the samples were taken out from aqueous dispersions, the hollow spheres were removed by the filtration, and the pollutant concentration was determined by spectrophotometry. The adsorption rate can be calculated using Eq. (3).

$$\text{Adsorption rate} = 100\% \times \frac{(C_0 - C)}{C_0} \quad (3)$$

Here, C_0 and C are the initial pollutant concentration and the residual pollutant concentration in the solution after adsorption, respectively.

3. Results and discussion

3.1. Morphology and structure of double-shelled WO_3@TiO_2 hollow spheres

Using methyl acrylate and sodium persulfate as surface active agents [32], PS spheres with smooth surfaces, negatively charged, and 380 nm diameter could be monodispersed, as shown in Fig. 1A. Tungsten cations from WCl_6 were adsorbed onto PS by electrical attractions, oxidized, and hydrolyzed. Fig. 1B showed a complete, uniform, and smooth WO_3 shell was formed and coated onto PS. The average diameter of PS@WO_3 core–shell particles was increased from 380 to 476 nm, so the thickness of WO_3 shell was 48 nm. After the hydrolysis of TBOT, a 12 nm titania layer was coated on the surface of PS@WO_3 particles, so the average diameter of PS@WO_3@TiO_2 core–shell particles was 500 nm and homogeneous in size (Fig. 1C). According to the results of TG and FTIR (Figs. 1s and 2s), the PS core could be removed by the calcination at 550 °C, only the stretch vibration bands of the W-O and O-Ti band were observed in WO_3@TiO_2 hollow spheres. The shell of hollow spheres was composed of WO_3 and TiO_2 and the atomic ratio of WO_3 and TiO_2 in

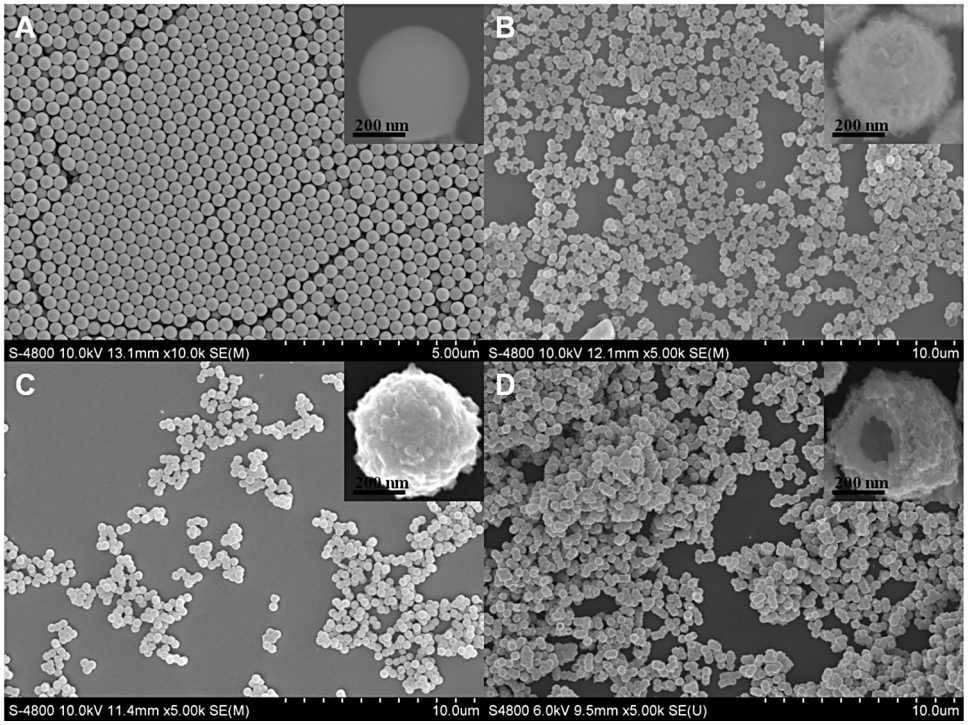

Fig. 1. SEM images of (A) PS spheres (380 nm), (B) PS@WO_3 core–shell nanocomposite particles (476 nm), (C) PS@WO_3@TiO_2 core–shell nanocomposite particles (500 nm), and (D) double-shelled WO_3@TiO_2 hollow spheres (470 nm).

double-shelled WO_3@TiO_2 hollow spheres were 38.31 and 7.89, respectively. The atomic ratios of WO_3 and TiO_2 in single-shelled WO_3-TiO_2 hollow spheres were 24.42 and 22.12, respectively (see Fig. 3s). The thickness and contents of WO_3 and TiO_2 layers could easily be tuned by modulating the concentrations of respective salts in reaction media. After calcination, monodisperse, porous, and intact WO_3@TiO_2 hollow spheres with a diameter of about 470 nm were obtained, which could be confirmed by the SEM image of a broken microsphere in Fig. 1D.

In agreement with SEM data (Fig. 2A), the TEM images of double-shelled WO_3@TiO_2 hollow spheres (Fig. 2B) confirmed that the produced particles were hollow and porous. A close inspection of the TEM image of WO_3@TiO_2 hollow spheres (Fig. 2C) revealed the presence of individual nanoparticles on a thick and layered shell. According to the SEM and TEM images of WO_3, TiO_2, single-shelled WO_3-TiO_2, and double-shelled WO_3@TiO_2 hollow spheres (see Fig. 4s), the morphology and structure of single-shelled WO_3-TiO_2 and double-shelled WO_3@TiO_2 were different. The HRTEM image of the nanocomposite showed four types of intimately contacted lattice fringes, confirming the formation of the junction between WO_3 and TiO_2 (Fig. 2D–G). The lattice spacings of 0.384 nm, 0.376 nm, and 0.363 nm were the interplanar distance between adjacent (0 0 2), (0 2 0), and (2 0 0) crystallographic planes of WO_3, while the lattice spacing of 0.351 nm matched that of the (1 0 1) plane of TiO_2. The polycrystalline nature of these individual nanoparticles was also confirmed by the SAED measurements (Fig. 2H). The yellow and green colored areas shown in HAADF-STEM mapping image (Fig. 2I) indicated that WO_3@TiO_2 hollow spheres were the combination of "Ti" and "W" enriched areas, i.e., WO_3 shell and TiO_2 shell. In the elemental mapping images of WO_3@TiO_2, the distribution of Ti and W was hierarchical structure, suggesting that WO_3@TiO_2 was double-shelled hollow spheres. This result was different from the elemental mapping images of single-shelled WO_3-TiO_2 (see Fig. 5s).

The hollow spheres of double-shelled WO_3@TiO_2 and single-shelled WO_3-TiO_2 were investigated by XRD analysis and the results were shown in Fig. 3. The presence of six peaks of TiO_2 at 2θ = 25.22, 37.78, 47.94, 54.15, 54.96 and 62.69 were found. These peaks were respectively indexed to the (1 0 1), (0 0 4), (2 0 0), (2 1 1), (1 0 5) and (2 0 4) planes of TiO_2, which were in good

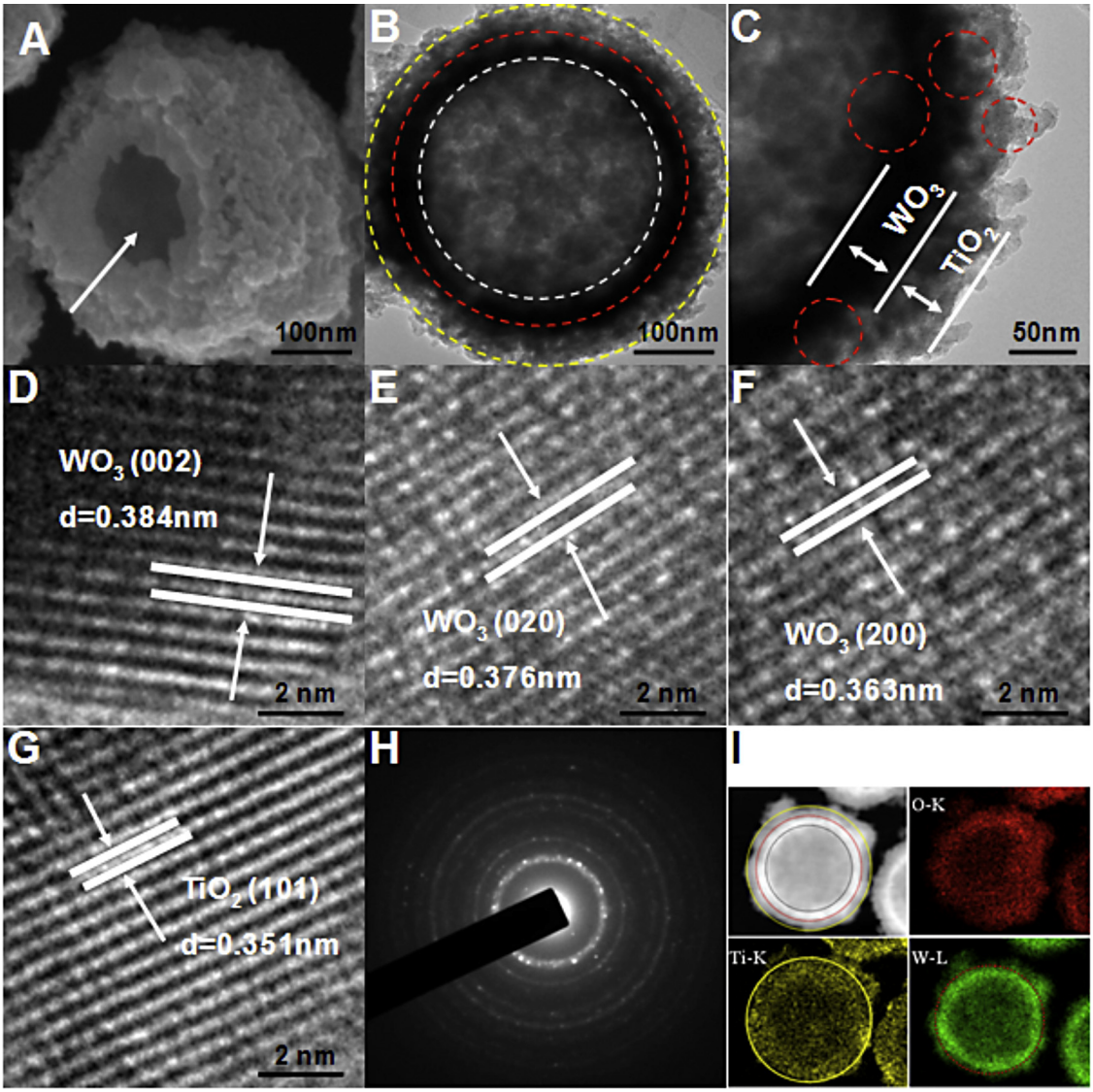

Fig. 2. (A) SEM images of double-shelled WO_3@TiO_2 hollow spheres, (B and C) TEM images of double-shelled WO_3@TiO_2 hollow spheres, (D, E, F and G) HRTEM images of double-shelled WO_3@TiO_2, (H) SAED images of double-shelled WO_3@TiO_2 hollow spheres, (I) HAADF-STEM mapping image of double-shelled WO_3@TiO_2 hollow spheres.

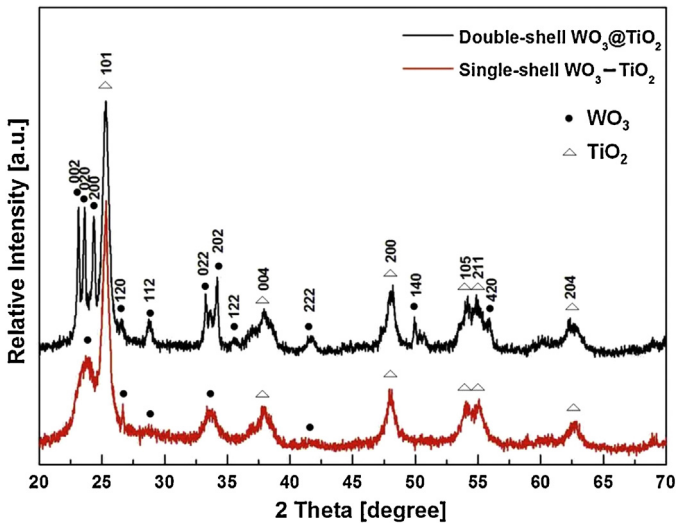

Fig. 3. XRD pattern of double-shelled WO_3@TiO_2 and single-shelled WO_3-TiO_2 hollow spheres.

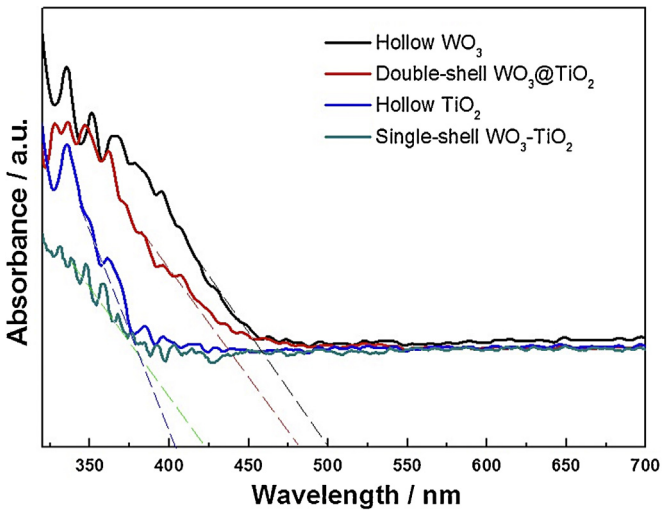

Fig. 4. Diffuse reflectance UV–vis spectra of hollow WO_3, hollow TiO_2, single-shelled WO_3@TiO_2, and double-shelled WO_3@TiO_2 hollow spheres.

agreement with the standard pattern of anatase titanium (JCPDS no. 21-1272) (see Fig. 6Bs). The 2θ peaks at 23.07, 23.59, 24.33, 26.58, 28.87, 33.20, 34.15, 35.67, 41.95 and 49.96, were corresponded to the diffraction from the (002), (020), (200), (120), (112), (022), (202), (122), (222), and (140) crystallographic planes of hexagonal monoclinic phase of WO_3 (JCPDS no. 43-1035) (see Fig. 6As). So the nanoparticles of TiO_2 and WO_3 in the shell wall were pure anatase and hexagonal monoclinic WO_3 phase, respectively.

The diffuse reflectance UV–vis spectra of the prepared photocatalysts were shown in Fig. 4. The absorption edges of pure TiO_2 and WO_3 hollow spheres were 400 and 500 nm, respectively, corresponding to the band gap of 3.2 and 2.7 ev. These results were similar to those reported in the literatures [33,34]. Because the nanoparticles of TiO_2 and WO_3 in the shell wall of WO_3@TiO_2 hollow sphere were pure anatase and hexagonal monoclinic WO_3 phase, respectively, the absorption edge of WO_3@TiO_2 hollow sphere was 480 nm. In the region of the solar spectrum, the light absorption of WO_3@TiO_2 hollow spheres was stronger than that of TiO_2 hollow sphere in sunlight light region (see Fig. 4), i.e., the visible light-harvesting efficiency of WO_3@TiO_2 hollow spheres was improved (Scheme 2).

3.2. Evaluation of photocatalytic and adsorptive activity

To investigate the effect of the structure of the photocatalysts on photocatalytic activity, five kinds of photocatalyst, including hollow WO_3, hollow TiO_2, P25, single-shelled WO_3-TiO_2, and double-shelled WO_3@TiO_2 hollow spheres, were used for the photodegradation of rhodamine B (or 4-nitroaniline, a cationic pollutant) and methyl orange (or trimesic acid, a anionic pollutant) under simulated sunlight irradiation for 75 min, and the results were shown in Fig. 5. Only 40.20% of rhodamine B could be photodegraded by P25. The photocatalytic activity of double-shelled WO_3@TiO_2 was higher than that of WO_3, TiO_2, P25, single-shelled WO_3-TiO_2. The photodegradation rate of rhodamine B by double-shelled WO_3@TiO_2 was 98.84%. Meanwhile, the linear relationship between $\ln(C_0/C)$ and t indicated that the photodegradation reactions followed pseudo-first-order kinetics (see Fig. 5) with rate constants (0.0098, 0.015, 0.0069, 0.028, and 0.058 min^{-1}) and

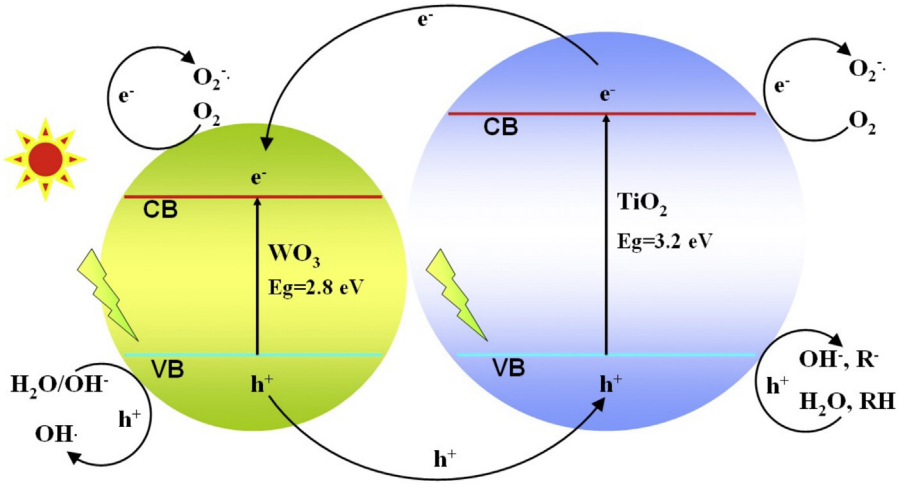

Scheme 2. The charge-transfer process in the monodisperse double-shelled WO_3@TiO_2 hollow spheres structures. After photon excitation by sunlight, photogenerated electrons (e^-) and holes (h^+) migrate to WO_3 and TiO_2, respectively, and react with the adsorbed species.

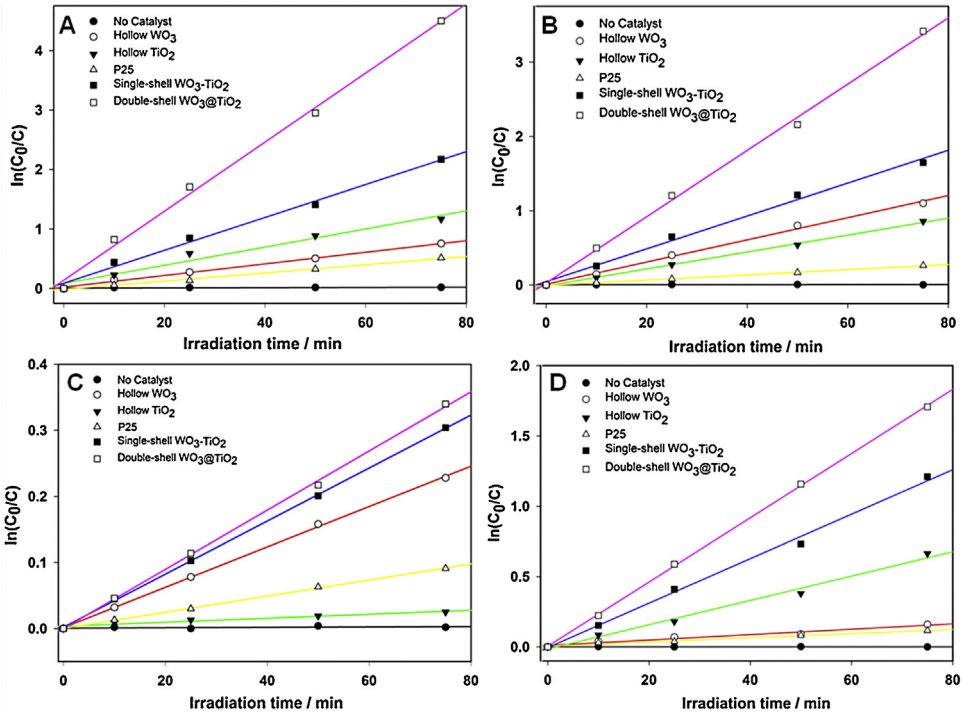

Fig. 5. Linear transform $\ln(C_0/C) = f(t)$ of the kinetic curves of (A) rhodamine B, (B) methyl orange, (C) 4-nitroaniline, or (D) trimesic acid photodegradation by double-shelled WO_3@TiO_2, single-shelled WO_3-TiO_2, TiO_2, WO_3 hollow spheres, or P25 under visible light irradiation.

Table 1
Visible light photodegradation rate constant k (min^{-1}) for WO_3, TiO_2, P25, single-shelled WO_3-TiO_2 and double-shelled WO_3@TiO_2 hollow spheres.

Sample	k (min^{-1})			
	Rhodamine B	Methyl orange	4-nitroaniline	Trimesic acid
WO_3	0.0098	0.015	0.0036	0.0019
TiO_2	0.015	0.011	0.0003	0.0087
P25	0.0069	0.0035	0.0012	0.0015
Single-shelled WO_3-TiO_2	0.028	0.022	0.0040	0.016
Double-shelled WO_3@TiO_2	0.058	0.045	0.0045	0.023

correlation coefficients R^2 (0.996, 0.969, 0.994, 0.992, and 0.996) for WO_3, TiO_2, P25, single-shelled WO_3-TiO_2, and double-shelled WO_3@TiO_2 hollow spheres, respectively. For comparison, the same procedure was also performed for other three kinds of aromatic pollutants (see Fig. 5, Table 1, and Table 1s).

The relative photocatalytic activity of the catalysts for the degradation of cationic and anionic aromatic pollutants was in the order of double-shelled hollow spheres WO_3@TiO_2 > single-shelled WO_3-TiO_2 > P25, i.e., the photocatalytic performance was improved by the coupling of TiO_2 with WO_3 (see Fig. 5 and Table 1). This synergistic effect could be attributed to the following reasons. The specific surface area, pore volume, and average pore size of WO_3@TiO_2 hollow spheres were 53.04 m^2/g, 0.1066 $cm^3\ g^{-1}$, and 8.042 nm, respectively (see Fig. 7s and Table 2s), indicating WO_3@TiO_2 hollow spheres was also a typical mesoporous materials. In the pH range of 2–5, the surface positively and negatively charged of double-shelled WO_3@TiO_2 hollow spheres were simultaneously present (see Fig. 6), which could enhance the affinity between photocatalyst and pollutants (including cationic and anionic aromatic pollutants) by electrostatic adsorption, and then the surface coverage and adsorption rate of pollutants onto the photocatalyst were increased. The double-shelled WO_3@TiO_2 exhibited higher adsorptive activity than WO_3, TiO_2, single-shelled WO_3-TiO_2, e.g., after adsorption 80 min, 97.58%, 68.79%, 9.89%, 58.24% of methyl violet could be adsorbed by double-shelled WO_3@TiO_2, WO_3, TiO_2 and single-shelled WO_3-TiO_2, respectively (see Fig. 7).

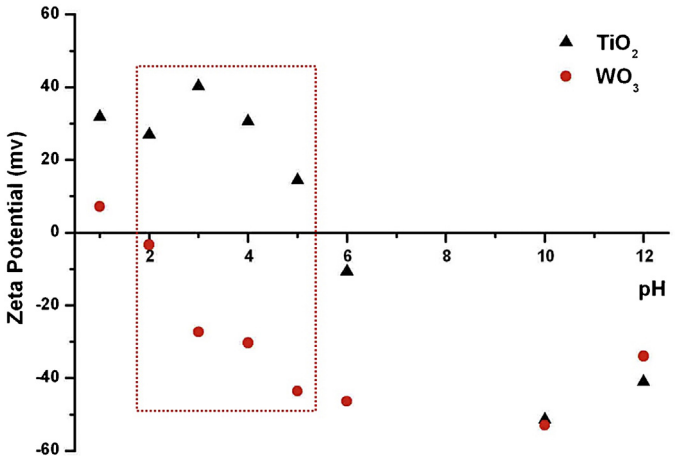

Fig. 6. Zeta potential of the TiO_2 and WO_3 hollow spheres at different pH.

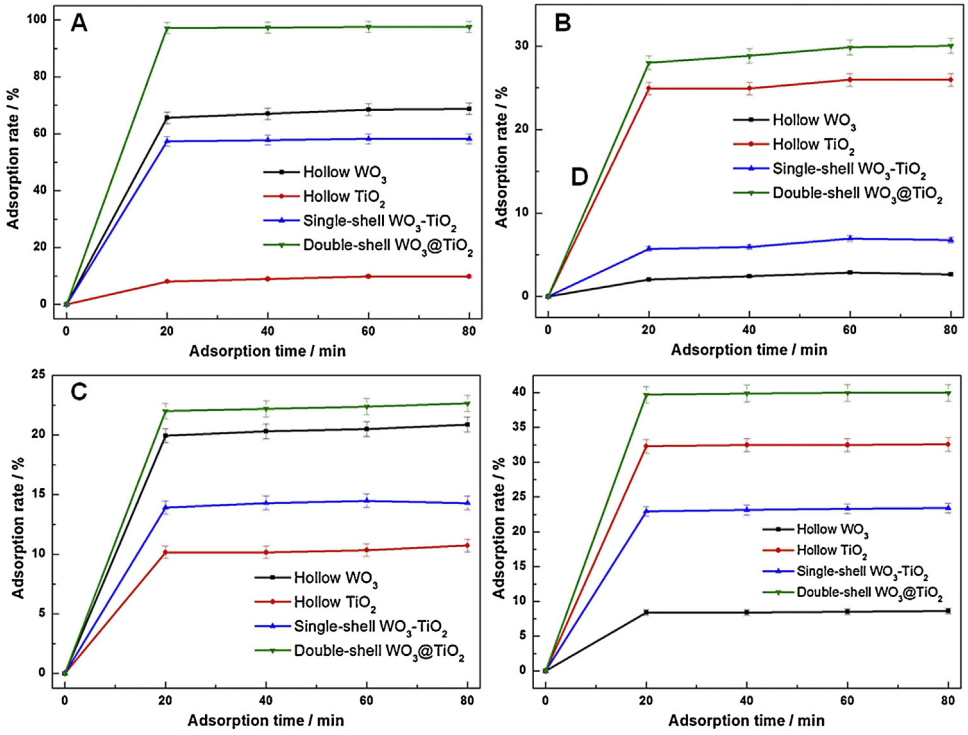

Fig. 7. Adsorption rate of (A) methyl violet (a cationic pollutant), (B) acid violet 43 (a anionic pollutant), (C) 4-nitroaniline (a cationic pollutant) and (D) trimesic acid (a anionic pollutant) on double-shelled WO_3@TiO_2, single-shelled WO_3-TiO_2, TiO_2 and WO_3 hollow spheres under dark.

4. Conclusions

In summary, we have demonstrated a novel and simple approach to fabricate of WO_3@TiO_2 and other heterojunction nanocomposite with double-shelled and 'positively and negatively charged', which could be used in environmental cleanup and electronic sensors. M_xO@N_yO hollow spheres could be the combination of metal oxide with different isoelectric point, including V_2O_5@TiO_2, WO_3@ZnO, WO_3@ZrO_2, WO_3@Ga_2O_3, V_2O_5@ZnO, V_2O_5@ZrO_2, and V_2O_5@Ga_2O_3 (see Table 3s).

Acknowledgments

This work is supported by the National Natural Science Foundation of China (20977074 and 21175115, S.X.L), the Program for New Century Excellent Talents in University (NCET-11 0904, S.X.L), Outstanding Youth Science Foundation of Fujian Province, China (2010J06005, S.X.L), and the Science & Technology Committee of Fujian Province, China (2012Y0065, F.Y.Z).

Appendix A. Supplementary data

Supplementary data associated with this article can be found, in the online version, at http://dx.doi.org/10.1016/j.apcatb.2014.05.021.

References

[1] X. Xu, C. Randorn, P. Efstathiou, J.T. Irvine, Nat. Mater. 11 (2012) 595–598.
[2] M.A. Shannon, P.W. Bohn, M. Elimelech, J.G. Georgiadis, B.J. Marinas, A.M. Mayes, Nature 452 (2008) 301–310.
[3] T.P. Yoon, M.A. Ischay, J. Du, Nat. Chem. 2 (2010) 527–532.
[4] R. Li, F. Zhang, D. Wang, J. Yang, M. Li, J. Zhu, X. Zhou, H. Han, C. Li, Nat. Commun. 4 (2013) 1432.
[5] S. Mubeen, J. Lee, N. Singh, S. Krämer, G.D. Stucky, M. Moskovits, Nat. Nanotechnol. 8 (2013) 247–251.
[6] W. Chen, Z. Fan, B. Zhang, G. Ma, K. Takanabe, X. Zhang, Z. Lai, J. Am. Chem. Soc. 133 (2011) 14896–14899.
[7] H. Zhang, X. Lv, Y. Li, Y. Wang, J. Li, ACS Nano 4 (2009) 380–386.
[8] J. Zhang, Q. Xu, Z. Feng, M. Li, C. Li, Angew. Chem. Int. Ed. 47 (2008) 1766–1769.
[9] O.K. Varghese, M. Paulose, T.J. LaTempa, C.A. Grimes, Nano Lett. 9 (2009) 731–737.
[10] L. Jing, W. Zhou, G. Tian, H. Fu, Chem. Soc. Rev. 42 (2013) 9509–9549.
[11] S. Li, J. Chen, F. Zheng, Y. Li, F. Huang, Nanoscale 5 (2013) 12150–12155.
[12] G.A. Parks, Chem. Rev. 65 (1965) 177–198.
[13] D. Chen, L. Gao, A. Yasumori, K. Kuroda, Y. Sugahara, Small 4 (2008) 1813–1822.
[14] G. Xi, B. Yue, J. Cao, J. Ye, Chem. -Eur. J. 17 (2011) 5145–5154.
[15] X. Chen, S.S. Mao, Chem. Rev. 107 (2007) 2891–2959.
[16] S. Shang, X. Jiao, D. Chen, ACS Appl. Mat. Interfaces 4 (2012) 860–865.
[17] T.L. Thompson, J.T. Yates, Chem. Rev. 106 (2006) 4428–4453.
[18] J. Yang, X. Zhang, H. Liu, C. Wang, S. Liu, P. Sun, L. Wang, Y. Liu, Catal. Today 201 (2013) 195–202.
[19] X.L. Yang, W.L. Dai, C. Guo, H. Chen, Y. Cao, H. Li, H. He, K. Fan, J. Catal. 234 (2005) 438–450.
[20] Y. Lu, M. Yuan, Y. Liu, B. Tu, C. Xu, B. Liu, D. Zhao, J. Kong, Langmuir 21 (2005) 4071–4076.
[21] G.F. Cai, X.L. Wang, D. Zhou, J.H. Zhang, Q.Q. Xiong, C.D. Gu, J.P. Tu, RSC Adv. 3 (2013) 6896–6905.
[22] Y.C. Nah, A. Ghicov, D. Kim, S. Berger, P. Schmuki, J. Am. Chem. Soc. 130 (2008) 16154–16155.
[23] B. Lu, X. Li, T. Wang, E. Xie, Z. Xu, J. Mater. Chem. A 1 (2013) 3900–3906.
[24] Y.C. Nah, N.K. Shrestha, D. Kim, P. Schmuki, J. Appl. Electrochem. 43 (2013) 9–13.
[25] W. Smith, A. Wolcott, R.C. Fitzmorris, J.Z. Zhang, Y. Zhao, J. Mater. Chem. 21 (2011) 10792–10800.
[26] W. Smith, Y. Zhao, J. Phys. Chem. C 112 (2008) 19635–19641.
[27] N.M. Vuong, D. Kim, H. Kim, J. Mater. Chem. C 1 (2013) 3399–3407.
[28] K. Lv, J. Li, X. Qing, W. Li, Q. Chen, J. Hazard. Mater. 189 (2011) 329–335.
[29] W. Leng, M. Chen, S. Zhou, L. Wu, Langmuir 26 (2010) 14271–14275.
[30] Y. Chen, C. Hu, X. Hu, J. Qu, Environ. Sci. Technol. 43 (2009) 2760–2765.
[31] J. Matos, J. Laine, J.M. Herrmann, Appl. Catal. B 18 (1998) 281–291.
[32] M. Agrawal, S. Gupta, A. Pich, N.E. Zafeiropoulos, J. Rubio-Retama, D. Jehnichen, M. Stamm, Langmuir 26 (2010) 17649–17655.
[33] G. Xi, Y. Yan, Q. Ma, J. Li, H. Yang, X. Lu, C. Wang, Chem. -Eur. J. 18 (2012) 13949–13953.
[34] X. Wu, Y. Tian, Y. Cui, L. Wei, Q. Wang, Y. Chen, J. Phys. Chem. C 111 (2007) 9704–9708.